International Core Journal of Engineering Volume 10 Issue 5, 2024
ISSN: 2414-1895 DOI: 10.6919/ICJE.202405_10(5).0061

Influence of Vibration Characteristics on the Wear of the Involute Spline Couplings in Aeroengines

Xiangzhen Xue*, Ning Zhang, Mingjie Shen, Wei Yu, Kuan Lin

Shaanxi University of Science and Technology, Mechanical and Electrical Engineering, 710021 Xi'an, China

*Corresponding author. E-mail address: xuexiangzhen@sust.edu.cn (X. Xue).

Abstract

To explore how vibration characteristics affect wear on involute splines in aeroengines, a finite element model of spline tooth face wear under different vibration characteristics was established using the Archard wear model, ALE adaptive grid technology, and the UMESHMOTION subroutine in Abaqus. The wear-depth variation law of the spline tooth face under different vibration amplitudes and vibration frequencies was analyzed. The findings indicate that with the increase in vibration amplitude and vibration frequency, the wear-depth of the spline coupling tooth face increases nonlinearly. The maximum wear-depth at tooth 1 amplitude of 50um is approximately 19 times that at 10um. Compared to the maximum wear-depth at 10 Hz, the maximum wear-depth at 50 Hz is 94% higher. The wear-depth of the spline tooth face along its axial location basically remains unchanged, slightly increasing at the axial middle position. The wear of the tooth's center portion is the least severe, while the wear of the tooth's bottom and tip are the most severe. The wear-depth of the spline coupling tooth face rises nonlinearly with an increase in vibration frequency and amplitude. This study provides a significant theoretical foundation for exploring the correlation between wear and vibration of involute spline systems in aero-engines and obtaining the self-diagnosis method of the wear fault of the system.

Keywords

Aero-engine Involute Spline; Vibration Amplitude; Vibration Frequency; UMESHMOTION Subroutine; The Archard Wear Model.

1. Introduction

In the aviation field, the involute spline coupling system plays a vital role in transmitting power within aircraft. the involute spline couplings system plays a crucial role in the power transmission of aircraft. Compared with the ground-light gas turbine spline, the involute spline in aircraft engines has the characteristics of light weight, high transmission speed, complex operating conditions, and environmental loads [1]. In addition, the wear issues of aero-engine splines are prevalent due to a variety of mechanical loads, including centrifugal force, constant torque, periodic torque, additional cyclic torque, transient peak torque, impact torque, misaligned load, and resonance. [2–3]. As reported by the Southwest Research Institute in the United States, more than 174 involute spline couplings are used in the United States Navy Black Hawk helicopter power transmission system, so the involute spline couplings are one of the key components of the aviation power transmission system. The reliability of the power transmission system is crucial for ensuring safety, and their safety and life improvement are tip priorities in air-craft engine design. Therefore, studying the influence of

ISSN: 2414-1895 DOI: 10.6919/ICJE.202405_10(5).0061

vibration characteristics on wear can help detect and diagnose wear faults in the aviation involute spline system in advance, thereby ensuring the normal operation and flight safety of the aircraft.

In recent years, scholars' research on aero-engine involute splines has basically focused on two aspects: on the one hand, Numerous studies have been carried out on the wear characteristics and anti-wear methods of aviation involute spline couplings; on the other hand, a detailed analysis has been made on the vibration characteristics of aviation involute spline couplings [4–5]. In terms of the wear characteristics and anti-wear methods of aircraft involute spline couplings, Francesca et al. [6–8] explored the wear damage conditions and wear reduction methods of spline couplings. Yuanqiang Tan et al. [9–10] analyzed the relative slip amount and contact pressure distribution law based on the single-pair mesh-spline tooth model and predicted spline wear with the Ruiz parameter method [11]. Investigating the fretting wear mechanism of aviation spline couplings, Xiangzhen Xue[12–15] et al. found that the fretting wear process includes several wear types, such as fatigue cracks and metal transfer phenomena. Sitai Yu [16] developed a finite element contact model for spline couplings with surface coatings and demonstrated that appropriate coating technology can enhance the wear resistance of splines. Guang Zhao et al.[17-18] provided a review of research on aviation splines from the aspects of failure modes, fatigue strength, surface contact stress, lubrication, and misalignment effects on wear, as well as experiments. Yuzhong Wu[19] found that the cracks formed inside brittle oxides and the nanoscale layered structure are the main reasons for the ultimate failure of fretting wear. In terms of vibration characteristics analysis of aviation involute spline couplings, Yachao Sun [20] revealed the coupling vibration mechanism of the gear spline system under non-uniform spline clearance conditions through a dynamic model and studied the support stiffness characteristics and wear evolution law of the spline pair under the action of dynamic gear meshing force. Xiangzhen Xue et al. [21–24] established a nonlinear dynamic model of aviation involute spline couplings and carried out a detailed analysis of the system vibration characteristics and dynamic behavior of aviation involute spline couplings, considering the involute tooth profile, multitooth engagement behavior, and non-moderate working conditions. Li Xiao et al. [25–26] investigated the impact of misalignment on the dynamic characteristics of spline couplings using an independent wear test bench. By applying time-frequency analysis, Xinxing Ma [27] developed a nonlinear dynamic model of a spline shaft system with a non-smooth friction contact and explored the relevant friction vibration and instability processes.

It was found that the above studies only focused on one of the wear or vibrations of involute splines, and the research results have been widely used in aviation transmission systems, marine power transmission systems, and automotive transmission systems. However, in fact, the geometric structure of the involute spline and its application situation lead to its very complex and special working conditions, so a specific pairing relationship exists between the wear and vibration of the involute spline, so it is necessary to combine the two to explore its change law. Therefore, this study focused on aero-engine involute spline couplings and adopted an adaptive finite element method. Based on the Archard wear model, the dynamic simulation problem of short-term spline wear was addressed by utilizing the UMESHMOTION subroutine developed in Abaqus and integrating ALE adaptive mesh technology. The finite element model of spline tooth face wear under different vibration characteristics was established, and the effect of spline vibration on wear was studied considering the mutual wear between contact tooth faces. This study can provide methods and ideas for the dynamic simulation of spline wear over a long period of time and provide an important theoretical basis for exploring the interaction mechanism between wear and vibration of involute spline couplings so as to establish the correlation between wear and vibration of aviation involute spline systems and obtain the self-diagnosis method of wear faults in systems. At the same time, it is also helpful to optimize the wear performance of the spline coupling by controlling vibration frequency and amplitude, so as to improve the reliability and life of the aero-engine involved spline couplings.

ISSN: 2414-1895 DOI: 10.6919/ICJE.202405_10(5).0061

2. Involute Spline Coupling Wear Prediction Using the Achard Equation and Abaqus

2.1 Model for Predicting Spline Wear Using the Archard Equation

According to preliminary statistics, there are about 100 kinds of calculation models about wear, and their respective scopes of application are different. At present, the wear model proposed by Archard is widely used in wear prediction. This study uses the Archard formula for the wear calculation of aviation splines. The classic Archard wear formula is based on the assumption that contact stress and relative sliding distance are the main factors affecting contact surface wear, which can be described as:

$$\frac{dV}{ds}=k\frac{W}{3H} \tag{1}$$

where V is the wear volume, mm^3; k is the wear coefficient, MPa^{-1}; W is the contact normal load, N; s is the relative slip distance, mm; H is the material hardness. Applying it to small local area wear, formula (1) can be described as:

$$h=kps \tag{2}$$

where h is the wear-depth, mm; $k = K / H$ is dimensional wear coefficient, mm^2/N; p is the contact pressure, Mpa.

In the finite element analysis of spline vibration wear, the continuous wear process needs to be discretized. This involves dividing the entire wear process into multiple wear increments. Additionally, it is assumed that during tooth face contact wear, the pressure and wear coefficient at each contact point remain constant within very small incremental steps. Consequently, the wear-depth at node i is considered to be a constant value:

$$h_{i,n} = h_{i,n-1} + kp_{i,n}\Delta s_{i,n} \tag{3}$$

where $h_{i,n}$ is the total wear-depth of node i at the Nth incremental step; $h_{i,n-1}$ is the total wear-depth of node i at the (n-1)th incremental step; $p_{i,n}$ is the contact pressure of node i at the Nth incremental step; $\Delta s_{i,n}$ is the relative slip displacement increment of node i at the Nth incremental step. Considering that redrawing the mesh after node wear will increase the calculation time cost, an assumption can be made to reduce the calculation cost. Assuming that the wear amount within ΔN meshing periods remains the same for each period, the total wear-depth of node i after undergoing ΔN meshing periods is calculated as follows:

$$h_{i,n} = h_{i,n-1} + \Delta N kp_{i,n}\Delta s_{i,n} \tag{4}$$

2.2 Construction of a Finite Element Model

The selected material for the involute spline coupling in this work is 18CrNi4A, with a Young's modulus of 210GPa, Poisson's ratio of 0.3, and a density of 7800 kg/m^3. Table 1 displays the spline's essential geometric parameters. In order to improve the accuracy of the finite element simulation and enable a successful simulation calculation, the model is divided into hexahedral mesh cells following finite rules. This approach allows for a reduction in the number of tetrahedral meshes and an increase in the number of hexahedral meshes. Considering that the tooth shape of the involute spline coupling

ISSN: 2414-1895 DOI: 10.6919/ICJE.202405_10(5).0061

is irregular, manual mesh partitioning can effectively optimize the meshing process. The selection for the mesh type is C3D8R.

Table 1. Parameters of involute spline coupling

Parameter	Numerical value
Number of teeth z	12
Modulus m/mm	1.5
Pressure Angle/(°)	30
Tooth width /mm	9
External spline aperture /mm	8
Internal splined journal /mm	25

In this work's finite element calculation, the primary focus is on the wear of the external spline. As such, the external spline is configured as the slave plane, while the internal spline is set as the main plane. For the contact process, the contact characteristics used are as follows: The normal behavior is hard contact, and the tangential behavior is modeled using a penalty function. The wear coefficient is specified as 0.2, and the slip mode considered is finite slip. In the Archard wear model, slip is the principal variable used to determine wear. Consequently, the accuracy of the wear model is influenced by the chosen increment size for wear. If the increment step is too large, it can lead to unstable results, while an excessively large displacement increment renders the calculation results invalid. Conversely, utilizing an overly small increment step leads to longer calculation times, compromising the purpose of optimization calculations. Therefore, in this analysis, the chosen analysis step size is 0.05.

The finite element model in this study utilizes the contact calculation between the internal and external splines as input data for simulation. The model is loaded in two steps. In the first load step, torque is applied to the external spline, and displacement constraints are enforced. Due to limitations in Abaqus software, the torque cannot be directly applied to the end face. Instead, it must be applied to a reference point. Therefore, a coupling constraint is set up in the interaction module, with the established RP1 as the control point and the end face of the external spline as the coupling plane. Finally, a torque of 50 N·m is applied at RP1, according to the actual engineering load. The load is gradually increased following an amplitude curve to reduce the number of iterations and achieve stable calculations. As for the displacement constraints, the translation degrees of freedom in the Z direction and the rotational degrees of freedom in the XY plane are constrained for the external spline, while the rotational degree of freedom around the axial direction Rz is released. The boundary conditions for the internal spline are relatively simple. A reference point RP2 is established at the origin and is rigidly coupled with all the elements of the internal spline. RP2 is set to be fully fixed. In the second load step, the translation degrees of freedom in the XYZ directions and the rotational degrees of freedom in the XYZ directions are constrained for the external spline, while the translation degrees of freedom in the YZ direction and the rotational degrees of freedom in the XYZ directions are constrained for the internal spline. Different amplitude and frequency sine wave cyclic vibration constraints are applied in the X direction. T The overall finite element model of a spline coupling is shown in Figure 1.

When using Abaqus finite element software for wear simulation, the movement of the contact node is calculated using the Archard wear formula. The movement direction of the contact node can be customized by the user, with the default being contact normal. This calculation is implemented through the UMESHMOTION user subroutine in Abaqus. However, it is important to note that when the amount of contact node movement is too large, such as in the case shown in Figure 1, mesh distortion and even negative volume phenomena may occur. This can have a significant impact on

ISSN: 2414-1895 DOI: 10.6919/ICJE.202405_10(5).0061

the accuracy of the finite element results. To address this, the affected cells need to be redrawn with a new mesh. In Abaqus, the mesh redrawing process is achieved using ALE (Arbitrary Lagrangian-Eulerian) adaptive mesh technology. ALE adaptive meshing combines the features of both pure Lagrange and Euler algorithms. This approach allows the mesh to flow independently from the material, maintaining mesh quality throughout the analysis without changing the original topology of the mesh.

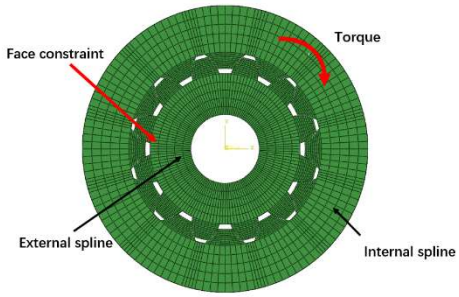

Figure 1. Finite element model of spline couplings and its boundary conditions

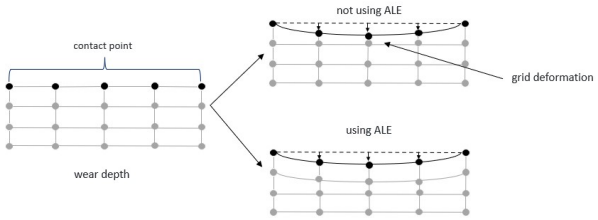

Figure 2. ALE adaptive grid technology

2.3 Wear Prediction of an Involute Spline Coupling based on the Achard Equation and Abaqus

Contact analysis is the foundation for the wear prediction of aircraft involved in spline couplings. In this case, Abaqus is used for the contact analysis. The accuracy of the solution depends on the discretization level of the model, the accuracy of the friction coefficient and wear coefficient, and the size of the increment step. The entire wear prediction process is as follows: First, a finite element model of the spline coupling system is established in the Abaqus software, and a suitable grid partition and boundary condition setting are performed on the model based on the mechanical structure and working conditions. Second, after the finite element model is established, static mechanics are solved. Through static mechanical analysis, the slip distance and contact stress distribution in the contact area of the spline coupling can be obtained. The contact stress and slip distance are the key parameters of the wear calculation. They reflect the magnitude of the force between the tooth faces and the degree of relative sliding. Then, based on the Archard wear model, the calculated contact stress and slip distance are used as input parameters, and the UMESHMOTION subroutine is used to actually calculate wear in the finite element model. In this process, it is necessary to combine ALE adaptive mesh technology to enable the model to automatically adjust the mesh during the wear process, thereby accurately simulating the evolution of wear. The specific implementation method is to measure the wear-depth of the outer spline surface node (ALE node) relative to the global coordinate system at specified intervals. In each substep of the analysis, the relative sliding is determined by calculating the relative displacement and contact stress (that is, the CPRESS value) of the outer spline surface node. And the wear distance is offset according to the vector direction given by the program. Finally, the nodes of the adaptive region adjust the mesh size and begin a new substep. The flow of the involute spline coupling wear calculation is presented in Figure 3.

ISSN: 2414-1895 DOI: 10.6919/ICJE.202405_10(5).0061

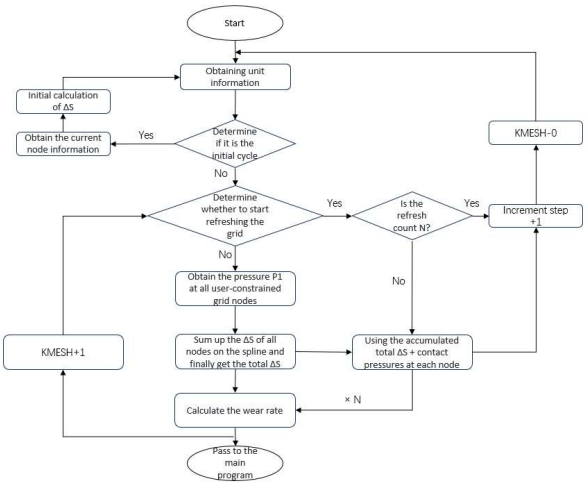

Figure 3. Wear prediction flow chart of an involute spline coupling using the Achard model and Abaqus

3. Wear Analysis of the Involute Spline Couplings under Different Vibration Characteristics

Since vibration amplitude and vibration frequency are the two most basic and important characteristics in the description of the vibration process, they have a direct and critical impact on the evaluation of wear and fatigue damage caused by vibration. In addition, vibration frequency and vibration amplitude are easy to measure and control parameters, so the two parameters of vibration amplitude and vibration frequency are selected in this work to research spline coupling wear.

As per the involute spline finite element model presented in Section 1.3, with corresponding boundary conditions and load settings, the wear coefficient $k=9.35e^{-08}mm^2/N$ is taken as the wear coefficient of spline vibration wear simulation by referring to literature, and the finite element model is finally solved. To gain a clearer understanding of the involute spline couplings' wear-depth modify rule, the serial number of the tooth of the external spline was marked. The serial number of the spline tooth is 1, which is upward on the X-axis, and the serial number of the spline tooth is 2, 3, 4...12, which is rotated counterclockwise, as displayed in Figure 4.

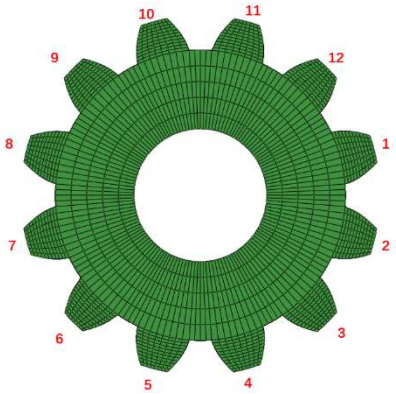

Figure 4. Number of external spline tooth faces

3.1 Analysis of Contact Characteristics of the Spline Coupling Tooth Face under Varied Vibration Amplitudes

3.1.1 Analysis of Contact Characteristics of the Spline Coupling Tooth Face under Varied Vibration Amplitudes

The contact stress is the most intuitive parameter to evaluate the contact strength of the tooth face, and it is also one of the main parameters to calculate the wear of the spline couplings. Figure 5 shows

ISSN: 2414-1895 DOI: 10.6919/ICJE.202405_10(5).0061

the distribution of contact stress on 12 tooth faces of the external spline when the vibration amplitude of the involute spline coupling in the X-axis direction is 10um, 30um, and 50um. The figure illustrates that the contact stress of the spline teeth numbered 4–8 is small, and the maximum contact stress of other spline teeth occurs in the middle of the tooth tip. This is because the spline is in the process of vibration; when the radial displacement reaches its maximum, the spline is in parallel misalignment, and the contact area of the tooth face is no longer evenly distributed but concentrated on the partially meshing teeth. When the amplitude is 10um, 30um, and 50um, respectively, the maximum contact stress is 121 MPa, 158 MPa, and 187 MPa, respectively. from which it can be concluded that the greater the amplitude, the greater the contact pressure of the tooth face.

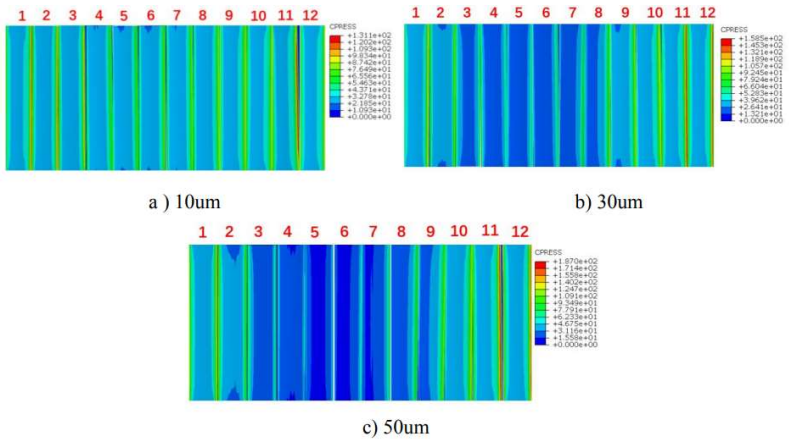

Figure 5. Distribution of contact stress on every tooth face at varying vibration amplitudes

Based on the cloud map depicting the distribution of contact stress for 12 spline teeth in Figure 5, As can be observed, splined tooth 1 has a greater contact stress than the other splined teeth. As a result, the distribution of contact stress under various amplitudes on the tooth face of tooth 1 is examined. Figure 6a) is the distribution curve of contact stress for spline tooth 1 along its axial location under different amplitude conditions, and Figure 6b) is the distribution curve of contact stress for spline tooth 1 along the radial position under different amplitude conditions. (Take the node at the tooth position in the axial position, and take the node at the torque input end in the radial position.).

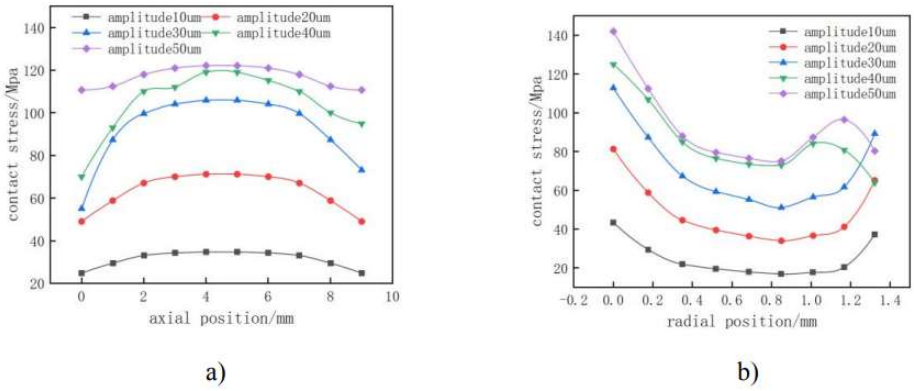

Figure 6. Distribution curve of contact stress for external spline tooth 1 under different amplitudes

As can be seen from Figure 6a, under different vibration amplitudes, the contact stress distribution curves along the axial position are convex; the tooth face's contact stress first increases and then decreases, and the contact stress at the axial position of 5mm is the largest. It can be seen from Figure 6b) that, under different vibration amplitude conditions, the contact stress distribution curve along the radial position is concave. The contact stress on the tooth face first decreases and then increases,

ISSN: 2414-1895 DOI: 10.6919/ICJE.202405_10(5).0061

and the contact stress at the bottom of the tooth is the largest. This is because the radial vibration brings intermittent impact and decreased load sharing, and the contact stress concentration at the spline tooth bottom is intensified. When the amplitude is 50um, the maximum contact on the tooth face should be 1.5 times the minimum contact stress.

3.1.2 Analysis of Spline Coupling Tooth Face Wear under Different Vibration Amplitude Conditions

By extracting the wear-depth at each node of the tooth face of spline tooth 1, the wear-depth distribution diagram of tooth 1 is obtained when the frequency is 40 Hz and the amplitude is 10 mm, 30 mm, and 50 mm, respectively (Figure 7). In the figure, it can be clearly seen that the wear-depth distribution of spline tooth 1 tooth face is 0.78um and 0.37um at the amplitude of 10um, and 3.77um and 1.94um at the amplitude of 50um. When the amplitude is 50um, the tooth face has a maximum wear-depth of 8.34um and a minimum wear-depth of 4.27um. These findings demonstrate that as vibration amplitude increases, so does the tooth face's wear-depth and the severity of the wear process.

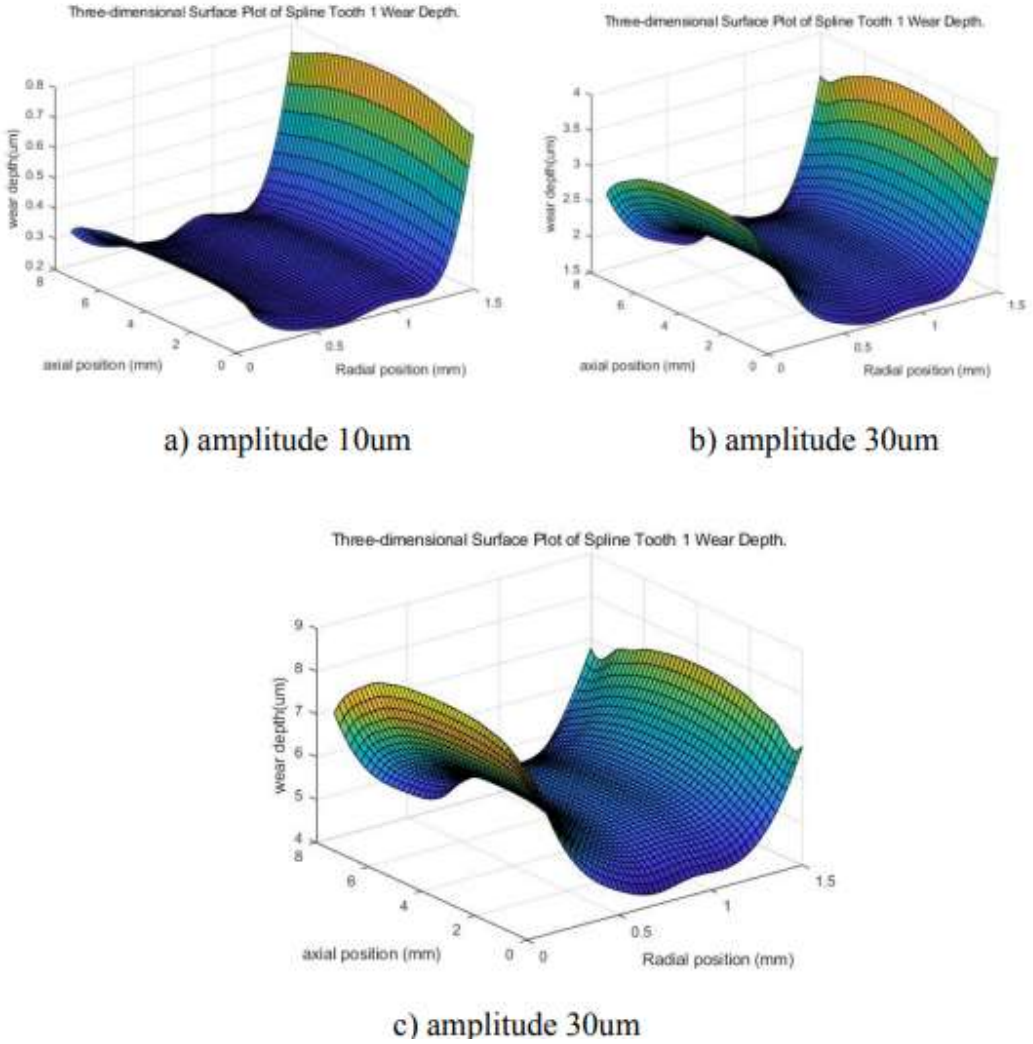

Figure 7. Wear-depth distribution of spline tooth face 1

Figure 8a) shows the distribution of wear-depth on spline tooth face 1 at axial position under different amplitudes, and Figure 8b shows the wear-depth distribution of spline tooth face 1 at radial position under different amplitudes.

ISSN: 2414-1895 DOI: 10.6919/ICJE.202405_10(5).0061

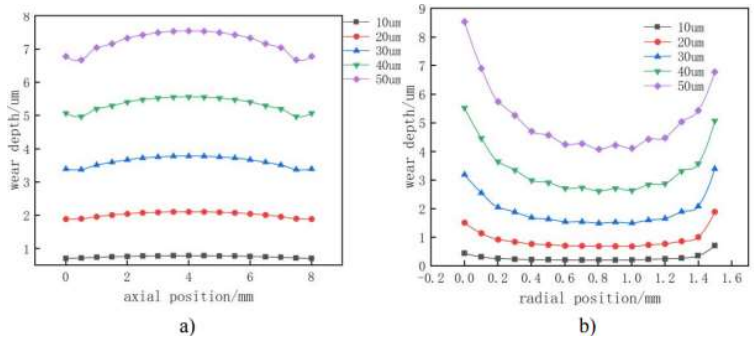

Figure 8. Distribution curve of wear-depth on the spline tooth face under different amplitudes

Figure 8a) shows that there is a little rise at the axial location of 3 ~ 6 mm, and otherwise the spline tooth face's wear-depth is largely unchanged along its axial position. The wear-depth of the tooth face increases as the vibration amplitude increases. The highest wear-depth occurs at 0.78um when the amplitude is 10um. As the amplitude grows, the wear-depth increases more and more, reaching 7.54um at 50um. Radial wear-depth on the tooth face is concave under varied amplitudes, as Figure 8b) demonstrates. The wear-depth at the bottom of the tooth is the biggest, followed by the wear-depth at the tip, and the lowest at the middle of the tooth. As the amplitude reaches 50um, the wear-depths are 8.53um at the bottom, 6.78um at the tip the tooth, and 4.56um in the middle of the tooth. Because the purpose of spline teeth is to transfer torque on the shaft, the tooth's bottom experiences higher stress and friction. Additionally, because small vibrations and impacts are easily produced during operation, the wear at the tooth's bottom will become more noticeable.

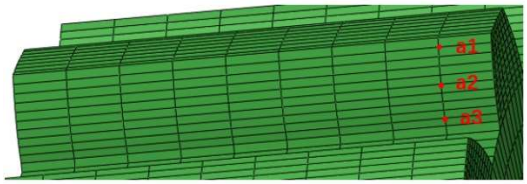

Figure 9. External spline local finite element model

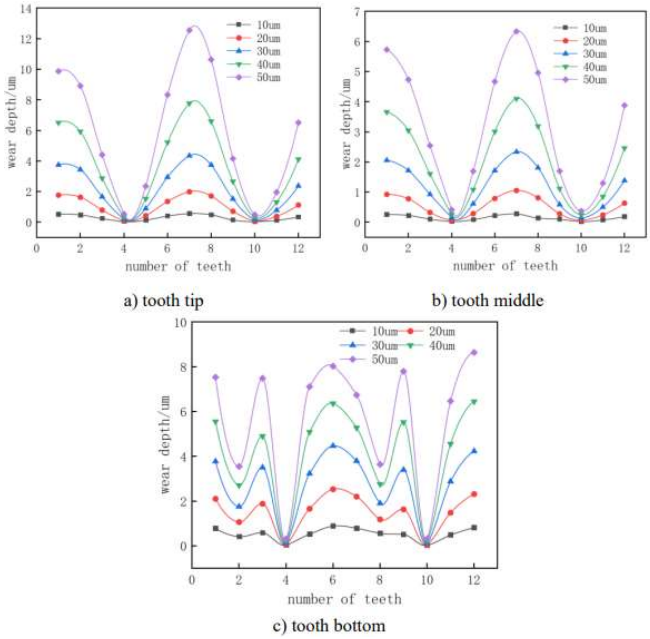

Figure 10. Wear-depth distribution on each exterior spline tooth face under different vibration amplitudes

ISSN: 2414-1895 DOI: 10.6919/ICJE.202405_10(5).0061

The spline wear-depth on different tooth faces is displayed in Figure 10 at a frequency of 40 Hz and a vibration amplitude between 10 and 50um. The tooth faces' wear-depth distributions at the crown, middle, and bottom of the teeth under varying amplitudes are shown in 10a), 10b), and 10c). The wear-depth distributions at various radial places are the three nodes a1, a2, and a3 in Figure 9 that are selected in the direction of the torque input end of the tooth face.

The wear-depth distribution of the external spline's tooth faces at varying amplitudes is displayed in Figure 10. At the tip of the tooth (Figure 10a), the distribution of wear-depth for every tooth is uneven, among which the wear-depth of No. 1, 7, and 12 teeth is larger, while that of No. 4 and 10 teeth is smaller. Because only x-axis vibration is used for the spline vibrational wear model, the spline wear-depth distributed near the x-axis is larger, while the spline wear-depth distributed near the y-axis is smaller. The theoretical analysis and the simulation results match. With the increase in vibration amplitude, the wear-depth of the tooth face increases. The wear-depth of No. 7 tooth is 0.56um when the amplitude is 10um, and 12.54um when the amplitude is 50um. Similar to the wear-depth distribution curve at the tooth's tip, the wear-depth distribution curve at the tooth's middle location (Figure 10b) shows a decrease in wear. The wear-depth of No. 7 tooth is 6.33um at the amplitude of 50um and 0.27um at the amplitude of 10um. Every tooth face's wear-depth at the tooth's bottom (Figure 10c) changes more unevenly. In contrast to the wear-depth distribution curve at the tooth's tip and middle, teeth No. 3 and No. 9 suddenly increase because the bottom part of the tooth is subjected to greater stress and friction, and it is easy to produce small vibrations and impacts during use, which will make the wear-depth distribution of each tooth at the bottom of the tooth change more unevenly. The No. 7 tooth has a wear-depth of 6.73um at 50um amplitude and 0.78um at 10um amplitude.

3.2 Analysis of the Spline Coupling Tooth Face's Wear-depth at Varying Vibration Frequencies

Analysis of contact characteristics of the spline coupling tooth face at varying vibration frequencies Figure 11 shows the contact stress distribution on 12 tooth faces of the external spline under the vibration frequencies of 20 Hz, 30 Hz, and 50 Hz.

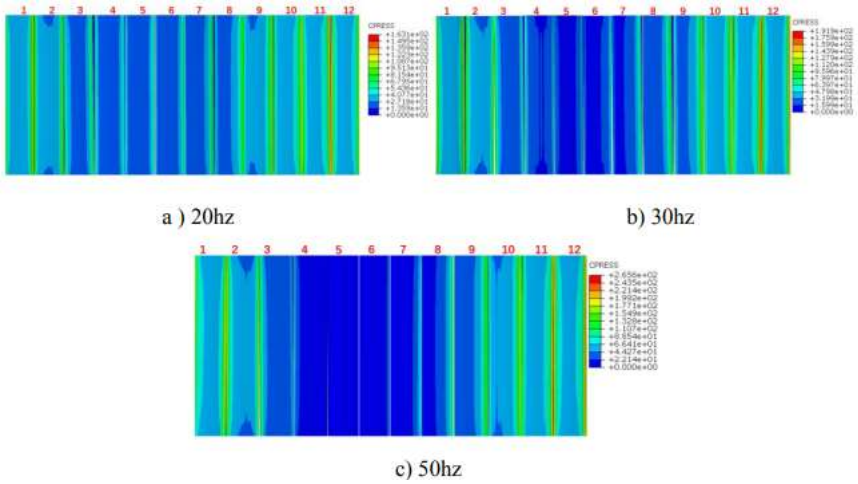

Figure 11. Distribution of contact stress on every tooth face at varying vibration frequencies

Figure 11 illustrates the unequal distribution of contact stress on the tooth face of each spline tooth, with a greater amount of contact stress at the tip and bottom of the tooth than at the middle. The spline teeth numbered 3–8 have minimal contact stress on their tooth faces, whereas the teeth numbered 1, 11, and 12 have significant contact stress. When the vibration frequency is 20 Hz, 30 Hz, and 50 Hz, the maximum contact stress is 163 MPa, 191 MPa, and 265 MPa, respectively. It can be concluded that the greater the vibration frequency, the greater the contact stress on the tooth face.

ISSN: 2414-1895 DOI: 10.6919/ICJE.202405_10(5).0061

Figure 12a)displays the spline tooth 1's axial distribution curve for contact stress under various frequency conditions, whereas Figure 12b)displays the contact stress radial distribution curve of spline tooth 1 under various frequency situations.

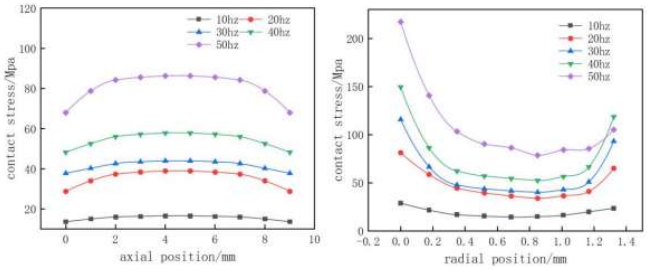

a) b)

Figure 12. Distribution curve of contact stress of external spline tooth 1 at different frequencies

Figure 12 makes it clear that the shape of the distribution curves of contact stress at axial and radial locations under different vibration frequencies is roughly the same as that at different vibration amplitudes. Based on Figure 12a), it is evident that the distribution curve of contact stress along the axial position presents a convex distribution under different vibration frequencies, and the maximum contact stress is 86.2 MPa when the frequency is 50 Hz. Figure 12b) illustrates how, at varying vibration frequencies, the contact stress distribution curve along the radial position exhibits a concave distribution, with the maximum contact stress occurring at the tooth bottom. The maximum contact stress at the tooth's bottom is 217.6 MPa at a frequency of 50 Hz.

3.2.1 Analysis of Spline Coupling Tooth Face Wear under Different Vibration Frequencies

The picture shows the wear-depth distribution of spline tooth face 1 at frequencies of 10 Hz, 30 Hz, and 50 Hz. The wear-depth distribution of spline tooth face 1 can be more clearly seen from the figure. The tooth face has a maximum wear-depth of 7.11um and a minimum wear-depth of 3.41um at a frequency of 10hz. The tooth face has a maximum wear-depth of 9.67um and a minimum wear-depth of 5.51um at a frequency of 30 Hz. The tooth face has a maximum wear-depth of 13.82um and a minimum wear-depth of 8.53um at a frequency of 50 Hz. These findings demonstrate that as vibration frequency increases, the tooth face's wear-depth increases and the wear process intensifies.

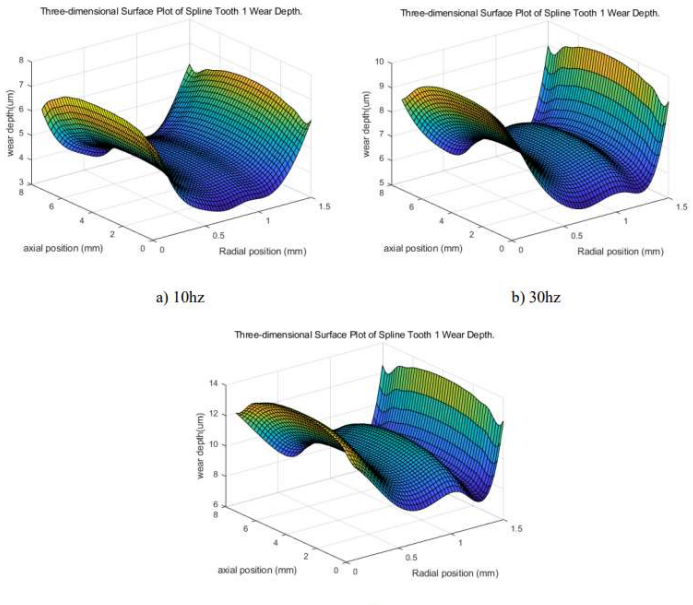

a) 10hz b) 30hz

c) 50hz

Figure 13. Distribution of wear-depth on the spline tooth face 1

ISSN: 2414-1895 DOI: 10.6919/ICJE.202405_10(5).0061

Figure 14a) displays the distribution of wear-depth on spline tooth face 1 at axial position under different frequencies, and figure 14b indicates the distribution of wear-depth on spline tooth face 1 at radial location under different frequencies.

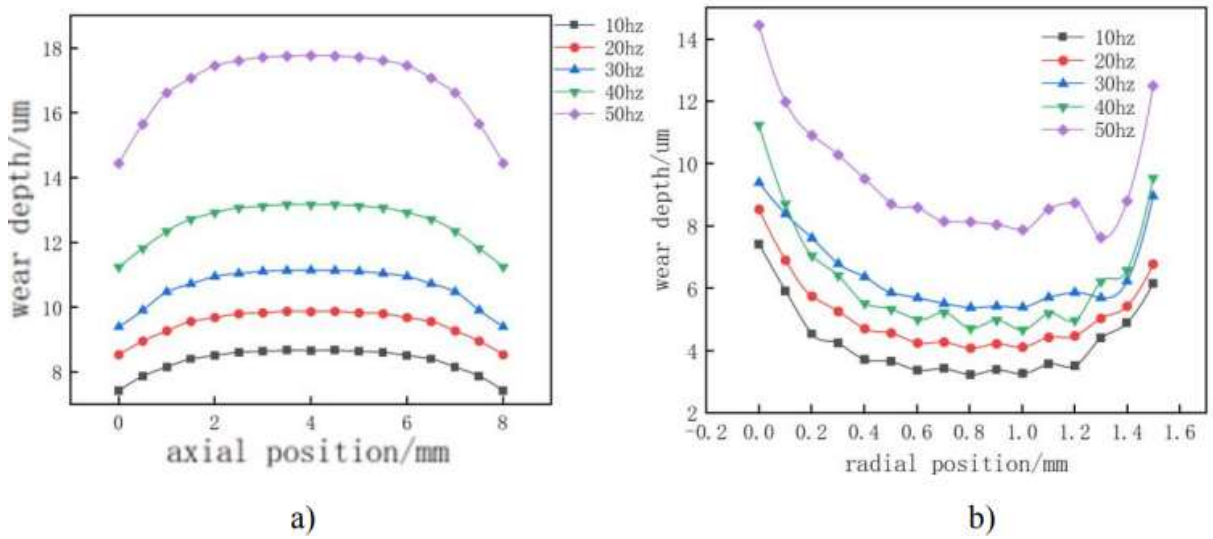

Figure 14. The spline tooth face's wear-depth distribution curve at various frequencies

As seen by Figure 14a, that the spline tooth face's wear-depth increases first, then decreases along its axial location, and slightly increases at its axial location of 3 ~ 6mm. The tooth face's wear-depth increases as the vibration frequency rises. The wear-depth stays within 8.33 um at a frequency of 10 Hz; when the frequency rises, the wear-depth increases noticeably. At a frequency of 50 Hz, the maximum wear-depth is 17.65 um. Figure b) illustrates this point: the tooth face's radial wear-depth is concave under various frequency conditions, with the greatest wear-depth occurring at the tooth's bottom, followed by the tip and middle portions of the tooth, respectively. The tooth's wear-depth at a frequency of 50 Hz is 14.44 um at the bottom, 12.49 um at the crown, and 8.58 um in the middle.

Figure 15 shows the wear-depth distribution of the spline on different tooth faces with a vibration frequency between 10 and 50 Hz when the vibration amplitude is 30 mm. 15a), 15b), and 15c) are the tooth face wear-depth distributions at different frequencies at the tip, middle, and bottom of the teeth, respectively. (The selection of nodes at the tip, middle, and bottom of each spline tooth is shown in Figure 10 above.).

Figure 15 shows the wear-depth distribution of the teeth faces of the external spline at different frequencies. Each tooth has an uneven wear-depth distribution at the tip (Figure 15a), with teeth Nos. 1, 7, and 12 having the largest wear-depths and teeth Nos. 4 and 10 having the lowest. The wear-depth of the teeth faces tend to grow as the vibration frequency increases. At 50 Hz, the No. 1 tooth's wear-depth is 14.41 um, while at 10 Hz, it is 7.4 um. At 50 Hz, the wear-depth is 94.7% more than at 10 Hz. The wear-depth distribution curve at the position in the middle of the tooth (Figure 15b) is similar to that at the tip the tooth, and the wear-depth decreases. The wear-depth of the No. 1 tooth at 50 Hz is 139% higher than that at 10 Hz. At the bottom of the tooth (Figure 15c), the wear-depth of each tooth face changes more unevenly. Compared with the wear-depth distribution curve at the tip and middle of the tooth, teeth No. 3 and No. 9 suddenly increase. The reason is that the contact pressure and shear force of the tooth face appear to increase stress concentration at the bottom of the tooth, and it is easy to produce small vibrations and impacts during use, which will make the distribution of wear-depth for every tooth at the bottom change more unevenly. Tooth 1 has 103% more wear-depth at 50 Hz than it does at 10 Hz.

ISSN: 2414-1895 DOI: 10.6919/ICJE.202405_10(5).0061

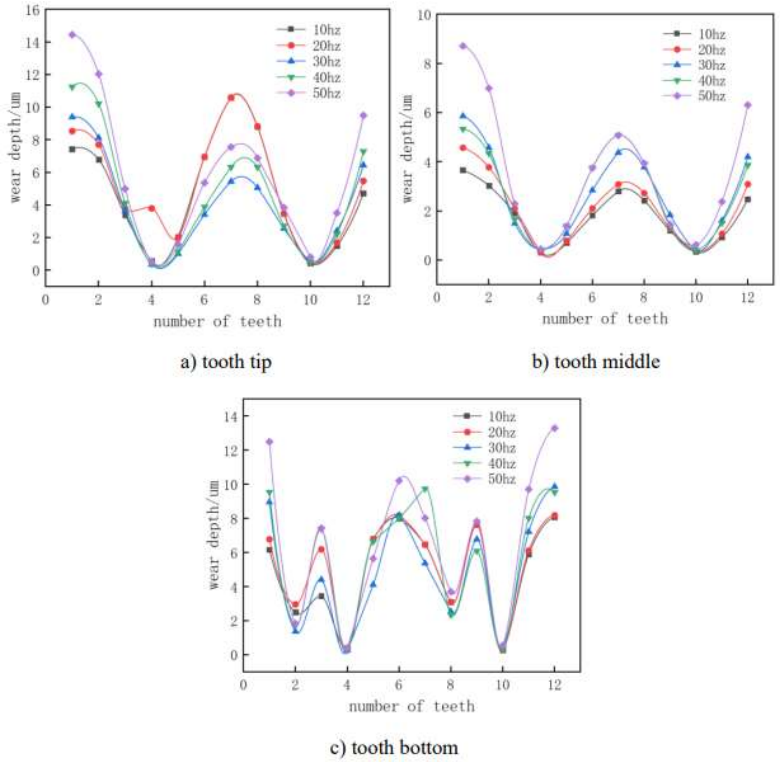

Figure 15. The exterior spline's wear-depth distribution on every tooth face at different vibration frequencies

4. Conclusion

Based on the Archard wear model, an adaptive finite element approach was used in this work, using Abaqus secondary development UMESHMOTION subroutine and ALE adaptive grid technology, to establish a spline tooth face wear finite element model under different vibration characteristics. Considering the mutual wear between contact tooth faces, the influence of spline vibration on wear is studied, and the relevant conclusions of the spline pair system under the given working conditions and geometric parameters are as follows:

1) An involute spline wear prediction method was proposed in this work, using the Achard model and Abaqus Based on the Archard wear model, the Abaqus secondary development of the UMESHMOTION subroutine combined with ALE adaptive mesh technology can simulate the evolution process of wear and improve the accuracy of wear calculation. This method can provide ideas for the wear failure of other parts, such as gears and bearings.

2) The wear-depth of the spline tooth face along its axial location is basically unchanged, and the wear-depth along the radial position is the largest at the bottom of the tooth, followed by the tip of the tooth, and the smallest in the middle of the tooth. When the amplitude is 50um, tooth1's maximum wear-depth is 8.53um.; when the amplitude is 10um, it is 0.44um. Compared to the maximum wear-depth at 10 Hz, the maximum wear-depth at 50 Hz is 94% higher.

3) The wear depth of each spline tooth grows non-linearly with increasing vibration amplitude and frequency at the tip, middle, and bottom. among them, teeth 1, 7, and 12 have the greatest wear-depths, while teeth 4 and 10 have smaller and may be disregarded wear-depths.

At the same time, the spline wear in this work is based on the static model without taking into account the shift in the actual contact area or the centrifugal force brought on by rotation. The selection of a vibration stroke comes from the larger value of engineering experience. In the simulation, factors such as temperature and lubrication are coupled to the friction coefficient and wear coefficient, which can further improve the simulation. In general, these findings provide an important theoretical foundation for the wear failure diagnosis of involute spline couplings in aeroengines and a method to

ISSN: 2414-1895 DOI: 10.6919/ICJE.202405_10(5).0061

optimize the wear performance by changing the amplitude and frequency, thereby improving the service life and reliability of spline couplings.

Acknowledgments

The authors are grateful for financial assistance from “Fundamental research on major projects for aero engines and gas turbines (Y2022-IV-0001-0018)”, Sichuan Science and Technology Program (2023YFG0201) and sponsored by the “The university youth innovation team of Shaanxi Province (2024)”.

References

[1] Q Hua, Q Zhou, Z Zheng, Z Dai, Y Ma and H Zhang. Assessment of Wear Form Weights in the Fretting Wear of Spline Couplings with BP Neural Network[J]. 2018 International Conference on Advanced Chemical Engineering and Environmental Sustainability (ICACEES 2018),2018,1:155-168.

[2] C Francesca, Q Waqar, M Andrea. A Methodological Approach for Incremental Fretting Wear Formulation[J]. Tribology Let-ters,2016,64(2):57-62.

[3] Conghui Chen. Common faults of aero-engine mechanical system [M]. Beijing: Aviation Industry Press, 2013:55-79.

[4] Q Hua, Q Zhou, Z Zheng, Z Dai, Y Ma and H Zhang. Assessment of Wear Form Weights in the Fretting Wear of Spline Couplings with BP Neural Network[J]. 2018 International Conference on Advanced Chemical Engineering and Environmental Sustainability (ICACEES 2018),2018,1:155-168.

[5] P Athir, P Blomqvist. Investigation of Wear in Spline Coupling for Saw Unit JPSR5500[D]. HALMSTAD UNIVERSITY,2019.

[6] C Francesca, Q Waqar, M Andrea. A Methodological Approach for Incremental Fretting Wear Formulation[J]. Tribology Let-ters,2016,64(2):57-62.

[7] C Francesca, M Andrea and P S d U Sevilla. Recent advances in spline couplings reliability[J]. Procedia Structural Integri-ty,2019,19:328-335.

[8] C Francesca, M Andrea. Methodology development of design a representative test specimen for wear damage in spline couplings[J].Procedia Structural Integrity,2018,8:204-211.

[9] Yuanqiang Tan, Li-Kuan Jiang, Shengqiang Jiang, et al. Micro-dynamic Friction Contact Analysis of Involute Splinecoupling [J]. Chinese Journal of Mechanical Engineering, 2018, 54(7): 123-130.

[10] Juanjuan Hu, Jianfa Hu, Yuanqiang Tan, et al. Research on Tooth Profile Modification of Involute Spline [J]. Journal of Me-chanical Strength, 2018, 40(1): 138-144.

[11] RUIZ C, BODDINGTON P, CHEN K. An investigation of fatigue and fretting in a dovetail joint[J]. Experimental Mechanics, 1984, 24(3): 208-217.

[12] Xue X, Li Y, Sui L, et al. Mechanism and prediction method of fretting damage in involute spline couplings of aero-engine[J]. Engineering Failure Analysis, 2023, 148: 107200.

[13] X Z Xue, Q X Huo, L Hong. Fretting wear-fatigue life prediction for aero-engine’s involute spline couplings based on ABAQUS[J]. Journal of Aerospace Engineering,2019,32(6):1-9.

[14] Xue X , Jia J , Huo Q ,et al. Experimental investigation and prediction method of fretting wear in rack-plane spline couplings:[J].Proceedings of the Institution of Mechanical Engineers, Part J: Journal of Engineering Tribology, 2021, 235(5):1025-1037.

[15] Xue X, Liu J, Jia J, et al. Prediction and Experimental Validation of Aviation Floating Involute Spline[J]. Lubricants, 2022, 10(10): 270.

[16] Sitai Yu. Simulation and Modeling of Anti-micro-motion Wear of Aviation Involute Spline Coating[D]. Beijing: Beijing Jiaotong University, 2021.

[17] Zhao G, Zhao X, Qian L, et al. A Review of Aviation Spline Re-search[J]. Lubricants, 2022, 11(1): 6.

[18] Guang Zhao, Shengxiang Li, Mei Guo, et al. Vibration Wear Pre-diction and Experiment of Aviation Spline[J]. Journal of Aerospace Power, 2018, 33(12): 2958-2964.

[19] Wu Y, Liang Y, Yin C, et al. Analysis of factors affecting the wear failure of an aeroengine spline pair and evolution mechanism of the tribolayer [J]. Engineering Failure Analysis, 2023, 146: 107113.

ISSN: 2414-1895 DOI: 10.6919/ICJE.202405_10(5).0061

[20] Sun Y, Shi J, Yang Y, et al. Dynamic modelling of gear–spline system with nonuniform spline clearance and wear evolution of spline[J]. Proceedings of the Institution of Mechanical Engineers, Part K: Journal of Multi-body Dynamics, 2023, 237(2): 236-260.

[21] Xue X, Huo Q, Dearn K D, et al. Involute spline couplings in aero-engine: Predicting nonlinear dynamic response with mass eccentricity[J]. Proceedings of the Institution of Mechanical Engi-neers, Part K: Journal of Multi-body Dynamics, 2021, 235(1): 75-92.

[22] Xue X, Liu J, Li Y, et al. Nonlinear dynamic analysis of floating involute splines considering comprehensive misalignment[J]. Journal of Sound and Vibration, 2023, 555: 117720.

[23] Xiangzhen Xue, Sanmin Wang, Ru Yuan. Nonlinear Dynamic Characteristics of Involute Spline Connection[J]. Journal of Harbin Institute of Technology, 2015, 47(01): 107-111.

[24] Qixin Huo, Jiahong Zheng, Xiangzhen Xue, et al. Analysis of Dynamic Meshing Force of Aviation Involute Spline Joint Considering Tooth Profile[J]. Science Technology and Engineering, 2019, 19(15): 111-117.

[25] Xiao L, Xu Y, Sun X ,et al. Experimental Investigation on the Effect of Misalignment on the Wear Failure for Spline Couplings[J].Engineering Failure Analysis, 2021.DOI:10.1016/j.engfailanal.2021.105755.

[26] Xiao L, Xu Y, Chen Z, et al. Non-linear dynamic response of misa-ligned spline coupling: Theoretical modeling and experimental investigation[J]. Journal of Vibration and Control, 2023, 29(7-8): 1590-1605.

[27] Ma X, Song Y, Cao P, et al. Self-excited vibration suppression of a spline-shafting system using a nonlinear energy sink[J]. International Journal of Mechanical Sciences, 2023, 245: 108105.